Journal of King Saud University – Science 35 (2023) 102397

HOSTED BY

Contents lists available at ScienceDirect

Journal of King Saud University – Science

journal homepage: www.sciencedirect.com

Original article

Masitinib analogues with the *N*-methylpiperazine group replaced – A new hope for the development of anti-COVID-19 drugs

Arun Bahadur Gurung [a,*], Mohammad Ajmal Ali [b], Reem M. Aljowaie [b], Saeedah M. Almutairi [b], Hiba Sami [c], Joongku Lee [d]

[a] Department of Basic Sciences and Social Sciences, North-Eastern Hill University, Shillong 793022, Meghalaya, India
[b] Department of Botany and Microbiology, College of Science, King Saud University, Riyadh 11451, Saudi Arabia
[c] Department of Microbiology, Jawaharlal Nehru Medical College and Hospital, Aligarh Muslim University, Aligarh 202002, India
[d] Department of Environment and Forest Resources, Chungnam National University, 99 Daehak-ro, Yuseong-gu, Daejeon 34134, Republic of Korea

ARTICLE INFO

Article history:
Received 26 May 2022
Revised 30 September 2022
Accepted 22 October 2022
Available online 31 October 2022

Keywords:
Masitinib
Masitinib analogues
N-methylpiperazine
SARS-CoV-2
Main protease inhibitors
COVID-19
Coronavirus
Molecular dynamics simulations

ABSTRACT

Masitinib is an orally acceptable tyrosine kinase inhibitor that is currently investigated under clinical trials against cancer, asthma, Alzheimer's disease, multiple sclerosis and amyotrophic lateral sclerosis. A recent study confirmed the anti-severe acute respiratory syndrome coronavirus 2 (SARS-CoV-2) activity of masitinib through inhibition of the main protease (M^{pro}) enzyme, an important pharmacological drug target to block the replication of the coronavirus. However, due to the adverse effects and lower potency of the drug, there are opportunities to design better analogues of masitinib. Herein, we substituted the *N*-methylpiperazine group of Masitinib with different chemical moieties and evaluated their drug-likeness and toxicities. The filtered analogues were subjected to molecular docking studies which revealed that the analogues with substituents methylamine in M10 (CID10409602), morpholine in M23 (CID59789397) and 4-methylmorpholine in M32 (CID143003625) have a stronger affinity to the drug receptor compared to masitinib. The molecular dynamics (MD) simulation analysis reveals that the identified analogues alter the mobility, structural compactness, accessibility to solvent molecules, and the number of hydrogen bonds in the native target enzyme. These structural alterations can help explain the inhibitory mechanisms of these analogues against the target enzyme. Thus, our studies provide avenues for the design of new masitinib analogues as the SARS-CoV-2 M^{pro} inhibitors.

1. Introduction

The COVID-19 pandemic has prompted global attempts to identify vaccines and specialized antiviral therapies as early as possible (Li and De Clercq, 2020; Zhang et al., 2020a). The main protease (M^{pro}, $3CL^{pro}$, nsp5) attracted a lot of interest among the coronaviral targets that have been investigated in the past, especially during the initial severe acute respiratory syndrome coronavirus (SARS-CoV) outbreak in early 2003 (Anand et al., 2003; Yang et al., 2003). Spike protein (S), RNA-dependent RNA-polymerase (RdRp, nsp12), NTPase/helicase (nsp13), and papain-like protease are other potential coronaviral targets (Hilgenfeld and Peiris, 2013; Wu et al., 2020a). The pp1a and pp1ab polyproteins encoded by the viral replicase gene are made up of distinct viral proteins that are required for replication (Wu et al., 2020b; Zhou et al., 2020). The processing of each polyprotein into distinct functional proteins is mediated by a chymotrypsin-like protease, 3CL M^{pro} or main protease (Mandal et al., 2021). The M^{pro} is necessary for viral replication, and its suppression prevents the production of mature virions (Ullrich and Nitsche, 2020). Therefore, the enzyme is an important target for the development of anti-SARS–CoV-2 therapeutic drugs (Jin et al., 2020; Mengist et al., 2021; Riva et al., 2020). SARS–CoV-2 M^{pro} is a cysteine protease that functions as a homodimer (Tong, 2002). It has a 96 percent amino acid sequence identity to the earlier SARS–CoV M^{pro}, and both enzymes have similar catalytic efficiency (Jin et al., 2020; Zhang et al.,

* Corresponding author.
E-mail address: arunbgurung@gmail.com (A.B. Gurung).
Peer review under responsibility of King Saud University.

Production and hosting by Elsevier

https://doi.org/10.1016/j.jksus.2022.102397
1018-3647/

2020b). The enzyme possesses three catalytic domains I, II and III (Zhang et al., 2020b) with the Cys145–His41 dyad in the catalytic site being aided by a water molecule hydrogen-bonded to the catalytic histidine (Anand et al., 2003; Kneller et al., 2020). The enzyme recognizes the sequence Leu-Gln↓Ser-Ala-Gly, where ↓ is the cleavage site but is promiscuous in its substrate sequence recognition. The active-site cavity can bind substrate residues at positions *P*1′-P5 in the substrate-binding subsites S1′–S5 (Kneller et al., 2020).

Masitinib is an orally accessible c-kit inhibitor (Dubreuil et al., 2009) that has been licensed for the treatment of mast cell malignancies in dogs (Hahn et al., 2008) and is being tested in humans for cancer (Ottaiano et al., 2017), asthma (Humbert et al., 2009), Alzheimer's disease (Folch et al., 2015), multiple sclerosis (Vermersch et al., 2012), and amyotrophic lateral sclerosis (Mora et al., 2020). Through disruption of the stem cell factor, mast cell c-Kit pathway, masitinib has direct antiproliferative effects on mast cells. Masitinib is a phenyl aminothiazole derivative that inhibits c-Kit as well as platelet-derived growth factors (PDGFR) α and β (Dubreuil et al., 2009; Le Cesne et al., 2010). Masitinib is also an inhibitor of the ATP binding cassette subfamily C member 10 (ABCC10) and ATP-binding cassette transporter G2 (ABCG2) transporters which substantially enhances paclitaxel intracellular accumulation *in vitro* (Kathawala et al., 2014a; Kathawala et al., 2014b) and furthermore, systemic administration of masitinib in combination with paclitaxel to mice inhibits the growth of xenografted tumors overexpressing the ABCC10 transporter (Kathawala et al., 2014b). Masitinib has also been shown to revert multi-drug resistance (MDR) in drug-resistant cancer cells to a normal condition. This process decreased doxorubicin drug resistance in canine cancer cells *in vitro*, but clinical trials have yet to validate it (Papich, 2016).

A recent study reported that Masitinib acts as a competitive inhibitor of M^{pro} as well and administration of masitinib to mice infected with SARS-CoV-2 shows a 200-fold decrease in viral titers in the lungs and nose, as well as reduced lung inflammation. Interestingly, this inhibitor was also effective against all of the identified variations of concern *in vitro* such as alpha (B.1.1.7), beta (B.1.351), and gamma (P.1) (Drayman et al., 2021). According to the X-ray crystallography study (PDB ID: 7JU7), Masitinib binds noncovalently between domains I and II of M^{pro} and inhibits the essential catalytic residues at the two active sites in the dimer. Mastinib has five distinct moieties: a pyridine ring, an aminothiazole ring, a toluene ring, a benzamide group, and an *N*-methylpiperzine group (Fig. 1). While the first four groups of Masitinib are involved in van der Waals, hydrophobic, and hydrogen bond interactions with the protease's catalytic residues, the role of the *N*-methylpiperazine group is unclear because it was discovered to be disordered and outside of the protease binding site. Given Masitinib's adverse effects, this study aims to replace the inhibitor's *N*-methylpiperazine group with other chemical moieties and investigate their toxicity using *in silico* techniques and their binding to M^{pro} using a molecular docking and dynamics approach. The key analogues proposed in this work are expected to have enhanced M^{pro} inhibitory activity with minimal adverse effects.

2. Materials and methods

2.1. Retrieval of structural analogues of masitinib

The structural analogues of masitinib with the *N*-methylpiperazine group replaced were retrieved from the PubChem database (Kim et al., 2016). The chemical structures of the

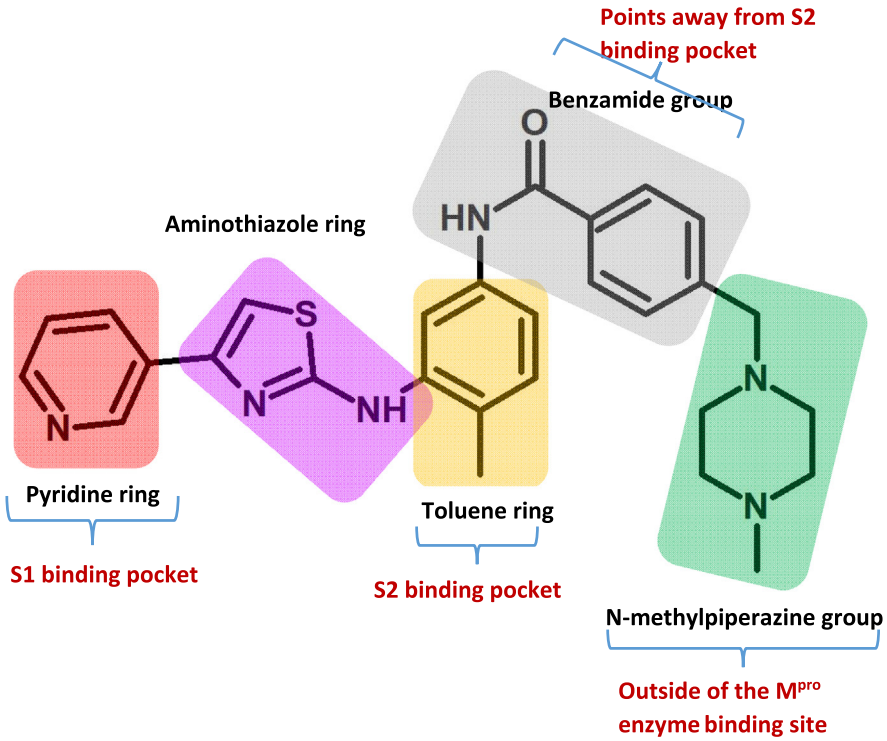

Fig. 1. Mastinib's chemical structure reveals five unique moieties: a pyridine ring, an aminothiazole ring, a toluene ring, a benzamide group, and an *N*-methylpiperzine group, all of which occupy different locations in the SARS-CoV-2 main protease enzyme, as shown by X-ray crystallography (PDB ID:7JU7).

Table 1
Drug-like properties of Masitinib and its analogues. The presence of an asterisk next to a molecule shows that it has passed drug-like filters and *in silico* toxicity assessments.

Compounds	PubChem CID	MW	cLogP	HBA	HBD	TPSA	RB	Druglikeness	Mutagenic	Tumorigenic	Reproductive Effective	Irritant
M1	10,023,927	400.505	5.3999	5	2	95.15	5	2.5987	none	none	none	none
M2*	10,074,640	498.653	4.7573	7	2	101.63	7	9.496	none	none	none	none
M3*	10,096,852	484.626	4.8344	7	2	101.63	6	8.6973	none	none	none	none
M4*	10,254,812	485.61	4.6479	7	2	107.62	7	3.8984	none	none	none	none
M5	10,319,726	416.504	4.4587	6	3	115.38	6	2.5237	none	low	none	none
M6*	10,319,727	416.504	4.986	6	2	104.38	6	2.6285	none	none	none	none
M7	10,341,171	404.468	5.1568	5	2	95.15	5	1.2587	none	none	none	none
M8	10,364,308	411.488	4.8916	6	2	118.94	5	−1.6813	none	none	none	none
M9	10,409,364	411.488	4.8916	6	2	118.94	5	−1.6813	none	none	none	none
M10*	10,409,602	415.52	4.0609	6	3	121.17	6	2.4492	none	none	none	none
M11	10,410,432	430.487	5.1674	7	2	113.61	5	2.5304	none	none	none	none
M12	10,412,398	469.611	5.4699	6	2	98.39	7	4.6983	none	none	none	none
M13*	10,453,738	402.477	4.7103	6	3	115.38	5	2.6065	none	none	none	none
M14*	10,476,173	401.493	4.3787	6	3	121.17	5	2.5785	none	none	none	none
M15	11,743,384	429.547	4.9524	6	2	98.39	6	3.4511	none	high	none	none
M16	42,613,483	471.54	4.3559	8	4	144.48	7	1.3641	none	none	none	none
M17*	42,625,974	444.514	4.969	7	2	121.45	7	0.27312	none	none	none	none
M18*	42,625,975	430.487	4.3707	7	3	132.45	6	2.5024	none	none	none	none
M19	42,626,345	445.502	4.0267	8	4	144.48	6	2.5065	high	none	none	none
M20	59,325,802	386.478	5.056	5	2	95.15	5	2.5987	none	none	none	none
M21*	59,651,299	429.547	4.4124	6	3	107.18	7	3.5815	none	none	none	none
M22*	59,789,379	429.547	4.9524	6	2	98.39	6	3.4511	none	none	none	none
M23*	59,789,397	471.583	4.725	7	2	107.62	6	3.6783	none	none	none	none
M24	59,789,404	444.558	5.1733	6	2	104.38	7	2.933	none	none	none	none
M25	74,821,251	471.54	4.3559	8	4	144.48	7	1.3641	none	none	none	none
M26	87,619,315	445.502	3.7976	8	4	158.47	6	3.0505	none	none	none	none
M27	91,443,299	400.505	5.3999	5	2	95.15	5	2.5987	none	none	none	none
M28	130,324,311	484.626	4.5044	7	3	110.42	7	5.0512	none	none	none	low
M29	140,528,385	459.529	4.074	8	4	144.48	7	3.2401	low	low	low	high
M30*	142,960,381	402.501	2.4009	6	4	122.42	5	2.4276	none	none	none	none
M31	142,964,721	415.52	4.703	6	3	107.18	6	3.0571	none	high	none	none
M32*	143,003,625	486.618	4.2939	7	2	112.2	7	3.6141	none	none	none	none
M33	144,600,411	400.505	5.3999	5	2	95.15	5	2.5987	none	none	none	none
M34	147,174,347	427.531	5.1157	6	2	107.51	6	3.2238	none	none	none	none
M35*	147,675,008	441.558	4.5218	6	3	107.18	5	2.9845	none	none	none	none
M36	149,779,171	485.531	5.2177	11	4	162.24	6	2.6318	none	none	none	none
M37*	151,845,207	415.52	4.0609	6	3	121.17	6	2.4492	none	none	none	none
M38*	152,130,115	483.595	4.9037	7	2	115.46	7	4.8315	none	none	none	none
M39*	154,499,650	429.503	4.1433	7	3	138.24	6	3.0372	none	none	none	none
Masitinib*	10,074,640	498.653	4.7573	7	2	101.63	7	9.496	none	none	none	none

analogues were downloaded in SDF format. The structures were optimized using the Merck molecular force field 94 (MMFF94) force field (Halgren, 1996) following steepest descent algorithm.

2.2. Physicochemical characteristics of the analogues

Lipinski's rule of five (ROF) (Lipinski, 2004), Veber's rule (Veber et al., 2002) filters and *in silico* toxicity tests such as mutagenicity, tumorigenicity, reproductive effects and irritancy were used to screen the analogues for drug-like qualities. The physicochemical features of the analogues were determined using the DataWarrior programme version 4.6.1 (Sander et al., 2015).

2.3. Retrieval of target protein structure

The atomic coordinates of the target enzyme the SARS-CoV-2 main protease were acquired from the protein data bank (PDB) (PDB ID: 7JU7). The X-ray crystal structure of the target enzyme complexed with masitinib has been determined at a resolution of 1.60 Å (Drayman et al., 2021).

2.4. Preparation of the analogues and target enzyme

Using AutoDock Tools-1.5.6, each analogue molecule was prepared for molecular docking by adding Gasteiger charges and hydrogen atoms, as well as appropriately determined torsions. The heteroatoms were removed from the target enzyme, which included ions, co-crystallized ligands, and water molecules. The requisite amount of polar hydrogen atoms and Kolmann charges were added to the target enzyme using the AutoDock Tools-1.5.6 tool.

2.5. Molecular docking studies

The Lamarckian genetic algorithm was used for molecular docking experiments, with docking parameters chosen from our previous publication (Gurung et al., 2020). For molecular docking, the AutoDock4.2 programme was utilised (Morris et al., 2009). A grid box with XYZ coordinates of 9.498, 4.128 and 20.681, a number of grid points of $70 \times 70 \times 70$, and grid spacing of 0.375 was chosen to determine the binding site of the analogues. Using a 2.0 root mean square deviation (RMSD) cut-off value, the docking positions were conformationally grouped. The LigPlot^{+} v 1.4.5 program was used to analyse the molecular interactions between analogues and the target enzyme (Laskowski and Swindells, 2011).

2.6. Molecular dynamics

The molecular docked protein–ligand complex structures were employed in GROningen MAchine for Chemical Simulations (GROMACS) 2019.2 software (Hess et al., 2008) with GROMOS96 43a1 force field to run MD simulations. The topologies for M^{pro} were built using the pdb2gmx utility included in GROMACS, while the ligand parameters were obtained using the PRODRG web server

Table 2
Binding energy and inhibition constant of masitinib and its analogues when docked against the SARS-CoV-2 main protease (M^{pro}) enzyme with an asterisk indicating the top three analogues.

Compounds	IUPAC Name	PubChem CID	Structure	Binding Energy (kcal/mol)	Inhibition constant (nM)
M3	4-(4-methylpiperazin-1-yl)-*N*-[4-methyl-3-[(4-pyridin-3-yl-1,3-thiazol-2-yl)amino]phenyl]benzamide	10,096,852	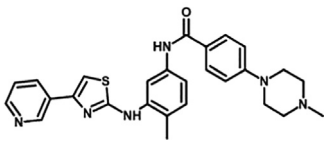	−8.93	285.58
M4	*N*-[4-methyl-3-[(4-pyridin-3-yl-1,3-thiazol-2-yl)amino]phenyl]-4-(morpholin-4-ylmethyl)benzamide	10,254,812	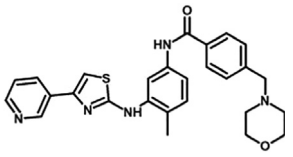	−9.50	108.40
M6	3-methoxy-*N*-[4-methyl-3-[(4-pyridin-3-yl-1,3-thiazol-2-yl)amino]phenyl]benzamide	10,319,727	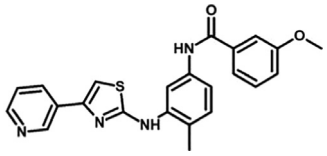	−9.61	90.87
M10*	4-(aminomethyl)-*N*-[4-methyl-3-[(4-pyridin-3-yl-1,3-thiazol-2-yl)amino]phenyl]benzamide	10,409,602	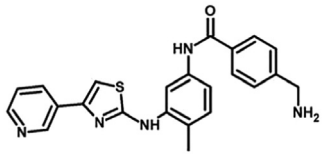	−10.50	19.98
M13	4-hydroxy-*N*-[4-methyl-3-[(4-pyridin-3-yl-1,3-thiazol-2-yl)amino]phenyl]benzamide	10,453,738	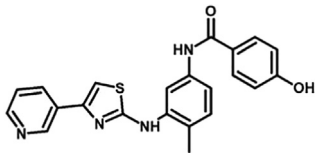	−9.03	241.50
M14	4-amino-*N*-[4-methyl-3-[(4-pyridin-3-yl-1,3-thiazol-2-yl)amino]phenyl]benzamide	10,476,173	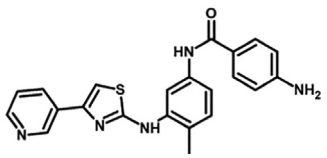	−8.80	351.81
M17	methyl 4-[[4-methyl-3-[(4-pyridin-3-yl-1,3-thiazol-2-yl)amino]phenyl]carbamoyl]benzoate	42,625,974	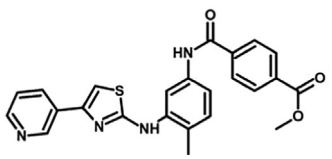	−9.39	130.88
M18	4-[[4-methyl-3-[(4-pyridin-3-yl-1,3-thiazol-2-yl)amino]phenyl]carbamoyl]benzoic acid	42,625,975	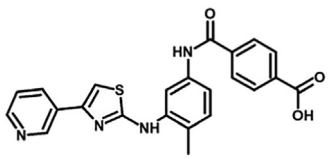	−9.16	192.99
M21	4-(methylaminomethyl)-*N*-[4-methyl-3-[(4-pyridin-3-yl-1,3-thiazol-2-yl)amino]phenyl]benzamide	59,651,299	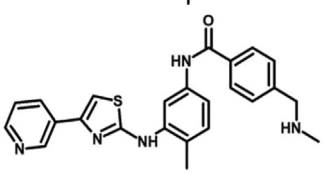	−9.75	71.32
M22	3-(dimethylamino)-*N*-[4-methyl-3-[(4-pyridin-3-yl-1,3-thiazol-2-yl)amino]phenyl]benzamide	59,789,379	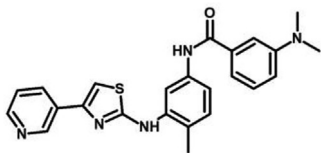	−9.53	102.81

Table 2 (*continued*)

Compounds	IUPAC Name	PubChem CID	Structure	Binding Energy (kcal/mol)	Inhibition constant (nM)
M23*	*N*-[4-methyl-3-[(4-pyridin-3-yl-1,3-thiazol-2-yl)amino] phenyl]-3-morpholin-4-ylbenzamide	59,789,397	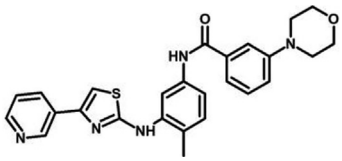	−10.10	39.26
M30	4-amino-*N*-[4-methyl-3-[(4-pyridin-1-ium-3-yl-1,3-thiazol-2-yl)amino]phenyl]benzamide	142,960,381	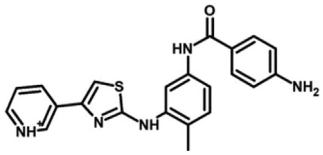	−8.55	539.20
M32*	[2-methyl-5-[[4-(morpholin-4-ylmethyl)benzoyl]amino] phenyl]-(4-pyridin-3-yl-1,3-thiazol-2-yl)azanium	143,003,625	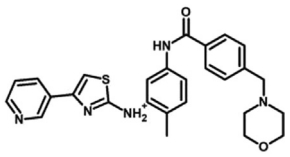	−9.94	51.70
M35	*N*-[4-methyl-3-[(4-pyridin-3-yl-1,3-thiazol-2-yl)amino] phenyl]-1,2,3,4-tetrahydroisoquinoline-7-carboxamide	147,675,008	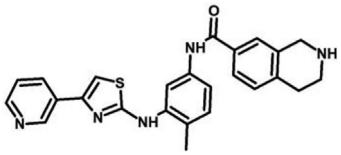	−9.78	68.23
M37	2-(aminomethyl)-*N*-[4-methyl-3-[(4-pyridin-3-yl-1,3-thiazol-2-yl)amino]phenyl]benzamide	151,845,207	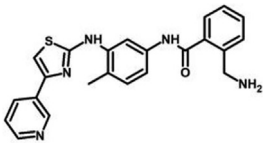	−9.55	99.37
M38	*N*-[4-methyl-3-[(4-pyridin-3-yl-1,3-thiazol-2-yl)amino] phenyl]-4-[(2-oxopyrrolidin-1-yl)methyl]benzamide	152,130,115	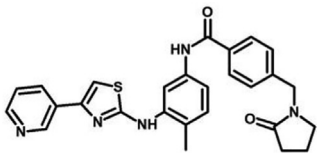	−9.13	203.85
M39	4-*N*-[4-methyl-3-[(4-pyridin-3-yl-1,3-thiazol-2-yl) amino]phenyl]benzene-1,4-dicarboxamide	154,499,650	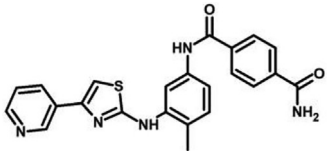	−9.81	64.85
Masitinib	4-[(4-methylpiperazin-1-yl)methyl]-*N*-[4-methyl-3-[(4-pyridin-3-yl-1,3-thiazol-2-yl)amino]phenyl]benzamide	10,074,640	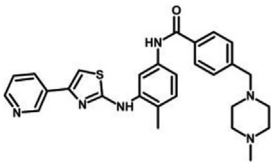	−9.72	74.64

(Schüttelkopf and Van Aalten, 2004). All the systems were centred in a triclinic box with a box-system distance of 1.0 nm and solvated with TIP3P water. 0.15 M NaCl was introduced to the M^{pro} system to neutralize the charge. The systems were then relaxed using the steepest descent method with 50,000 steps for energy minimization calculations at a tolerance value of 1000 kJ/mol/nm). The systems were then heated to 300 K using a Berendsen thermostat (Berendsen et al., 1984) with a coupling time of 0.1 ps, and the pressure was maintained with a coupling to a reference pressure of 1 bar, followed by equilibration with position restraint on the protein and ligand molecules for 0.1 ns using NVT (Number of particles, Volume, and Temperature) and NPT (Number of particles, Volume, and Temperature) ensembles. A smooth force-switch 1.2 nm cutoff was used in short-range interactions for energy minimization, NVT, and NPT relaxation simulations, and long-range electrostatics were evaluated using the PME (Particle-Mesh-Ewald) (Darden et al., 1993); additionally, hydrogen-bonds were restrained with the LINCS algorithm (Hess et al., 1997). Final MD simulations of 100 ns were run without constraints with a 2-fs integration time-step, and 1 ps trajectory snapshots were taken.

3. Results

We found thirty-nine structural analogues of masitinib, using a sub-structure search methodology against the PubChem database. Following that, drug-like filters such as ROF, veber's rule, and tox-

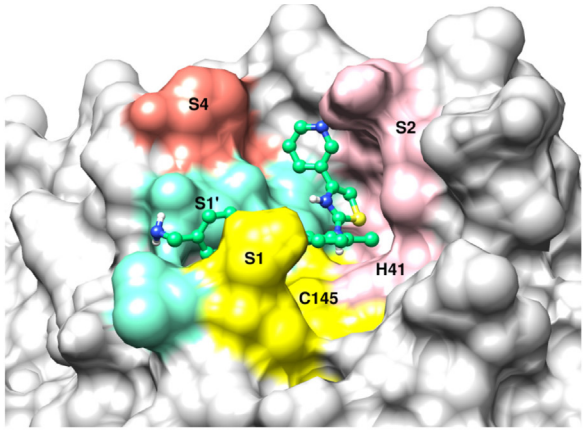

M10

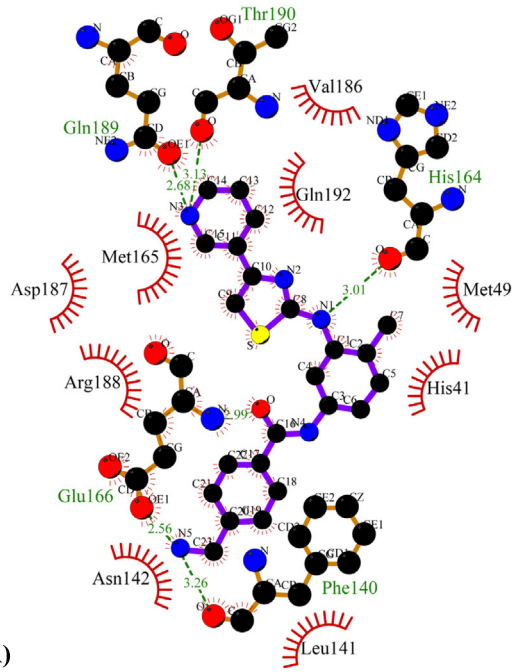

(A)

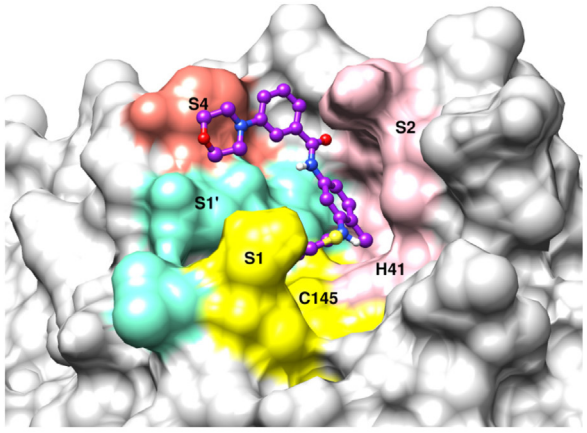

M23

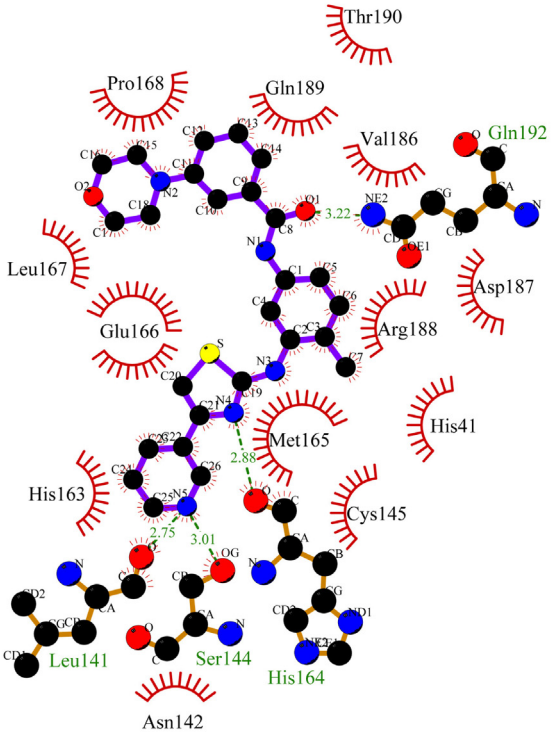

(B)

Fig. 2. The binding orientations and molecular interactions between SARS-CoV-2 M^{pro} enzyme and compounds (A) M10 (B) M23 (C) M32 and (D) Masitinib. Compounds in the active site pocket of the enzyme with catalytic dyad (His41 and Cys145) and substrate binding subsites-S1, S1′, S2 and S4 are shown in the binding models on the left side panel. The right-hand panel displays the LigPlot + program's molecular interaction data, with hydrophobic interactions depicted as semi-arcs with red eyelashes and hydrogen bonds depicted as green dashed lines.

icity filters were applied to these hits. A total of 18 analogues out of 39 were chosen for molecular docking experiments because they have the most favourable drug-like characteristics (Table 1). The analogue M10 binds to the SARS-CoV-2 main protease enzyme with a binding energy of −10.50 kcal/mol and inhibition constant of 19.98 nM (Table 2) and exhibits five hydrogen bonds with Phe140, His164, Glu166, Gln189 and Thr190, and hydrophobic interactions with His41, Met49, Leu141, Asn142, Met165, Val186, Asp187, Arg188 and Gln192 (Fig. 2**A**). The analogue M23 binds to the target enzyme with a binding energy of −10.10 kcal/mol and inhibition constant of 39.26 nM (Table 2) and shows four hydrogen bonds with Leu141, Ser144, His164 and Gln192 and hydrophobic

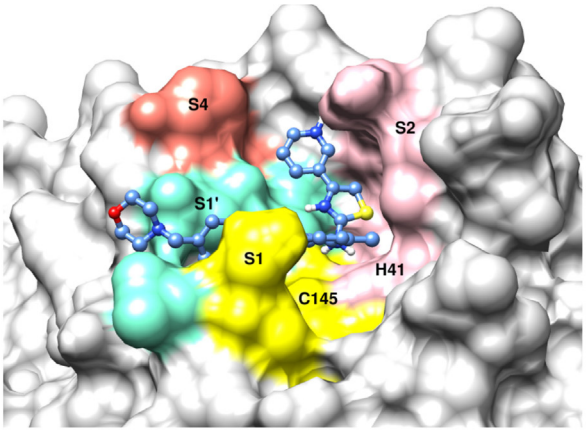

M32

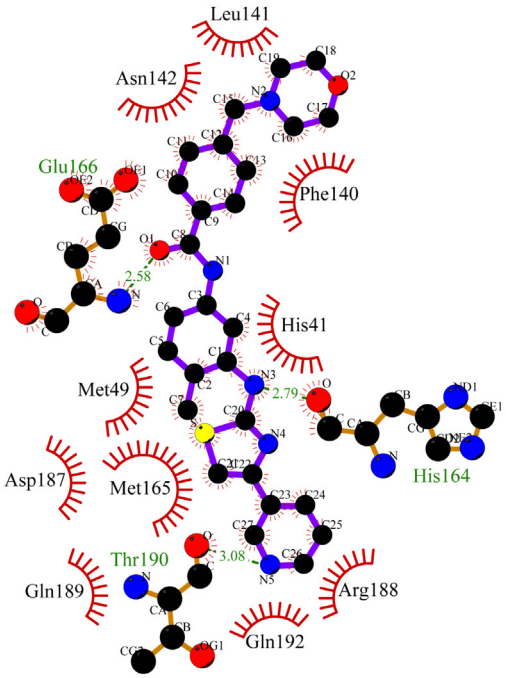

(C)

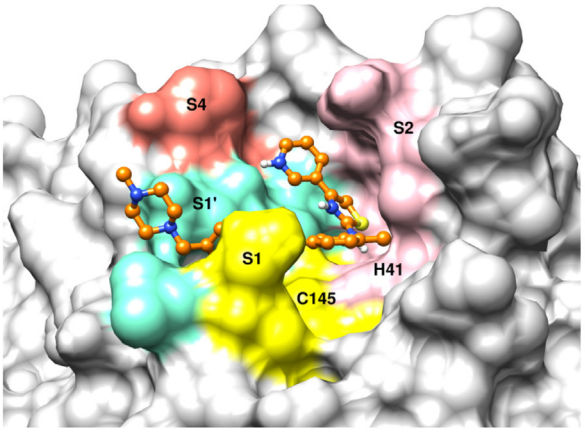

Masitinib

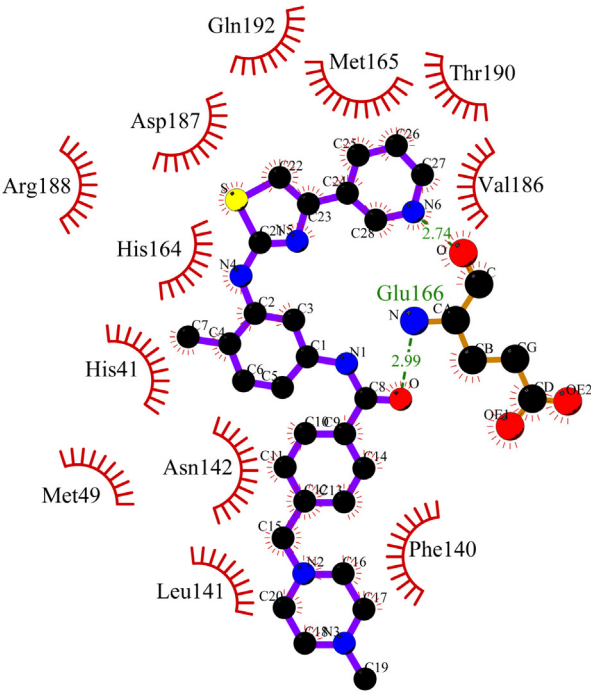

(D)

Fig. 2 (*continued*)

interactions with His41, Asn142, Cys145, His163, Met165, Glu166, Leu167, Pro168, Val186, Asp187, Arg188, Gln189 and Thr190 (Fig. 2**B**). The analogue M32 binds to the protease enzyme with a binding energy of −9.94 kcal/mol and inhibition constant of 51.70 nM (Table 2) and shows three hydrogen bonds with His164, Glu166 and Thr190 and hydrophobic interactions with His41, Met49, Phe140, Leu141, Asn142, Met165, Asp187, Arg188, Gln189 and Gln192 (Fig. 2**C**). Masitinib shows binding energy of −9.72 kcal/mol and inhibition constant of 74.64 nM (Table 2). The compound forms two hydrogen bonds with Glu166 and hydrophobic interactions with His41, Met49, Phe140, Leu141, Asn142, His164, Met165, Val186, Asp187, Arg188, Thr190 and Gln192 (Fig. 2**D**).

The unbound M^{pro} and complexes of the top 3 ranked analogues-M10, M23 and M32 were taken further for 100-ns MD simulations to understand the changes in structural properties (Table 3) of the target enzyme. M^{pro}, M^{pro}_M10, M^{pro}_M23 and M^{pro}_32 complexes have an average root-mean-square deviation (RMSD) of 0.332583 731 ± 0.041627085 nm, 0.295749208 ± 0.051314569 nm, 0.42903 9348 ± 0.05700657 nm and 0.207552255 ± 0.022640365 nm

Table 3
Average structural properties of unbound SARS-CoV-2 main protease (M^{pro}) and M^{pro}-analogue docked complexes.

Systems	RMSD (nm) Protein	Ligand	Rg (nm)	SASA (nm^2)	Hydrogen bonds Protein	Ligand
M^{pro}	0.332583731± 0.041627085		2.127997± 0.017467845	127.0979391± 6.538834755	211.5834166± 9.206371963	
M^{pro}_M10	0.295749208± 0.051314569	0.314784896 ± 0.058489328	2.120922877 ± 0.021329819	128.082026 ± 5.499573972	214.5474525 ± 8.729604573	2.934065934 ± 1.31516096
M^{pro}_M23	0.429039348 ± 0.05700657	0.710852126 ± 0.203861157	2.148384565 ± 0.021399429	136.912978 ± 2.469146035	207.3446553 ± 7.46713425	1.23976024 ± 1.145625394
M^{pro}_M32	0.207552255 ± 0.022640365	0.27076158 ± 0.065500399	2.225106244 ± 0.013538302	146.066041 ± 4.0438426	219.1978022 ± 8.291009297	2.094905095 ± 0.839037553

respectively (Table 3). The binding of the analogues decreases the flexibility of the target enzyme except for M23 (Fig. 3). The average RMSD values of M10, M23 and M32 were 0.314784896 ± 0.05848 9328 nm, 0.710852126 ± 0.203861157 nm and 0.27076158 ± 0.065500399 nm. The root-mean-square fluctuation (RMSF) plot was generated to evaluate the residue-wise fluctuations in the target enzyme before and after the binding of the analogues. (Fig. 4). The radius of gyration (Rg) of unbound M^{pro} and M^{pro}- analogue complexes was plotted to explore their structural compactness (Fig. 5). The Rg values for M^{pro}, M^{pro}_M10 M^{pro}_M23 and M^{pro}_32 complexes were 2.127997 ± 0.017467845 nm, 2.120922877 ± 0.021329819 nm, 2.148384565 ± 0.021399429 nm and 2.2251062 44 ± 0.013538302 nm respectively. The Rg plot suggests that the analogues induce conformational changes in M^{pro} leading to decreased structural compactness except for M10. The solvent-accessible surface area (SASA) analysis for unbound M^{pro} and M^{pro} docked complexes was performed (Fig. 6). The average SASA values for M^{pro}, M^{pro}_M10 M^{pro}_M23 and M^{pro}_M32 complexes were determined to be 127.0979391 ± 6.538834755 nm^2, 128.082026 ± 5.499573972 nm^2, 136.912978 ± 2.469146035 nm^2 and 146.0660 41 ± 4.0438426 nm^2 respectively. The formation of hydrogen bonds during the simulation were computed for unbound M^{pro} and M^{pro} docked complexes (Fig. 7**A**). M^{pro}, M^{pro}_M10 M^{pro}_M23 and M^{pro}_M32 complexes exhibit an average number of intramolecular hydrogen bonds of 211.5834166 ± 9.206371963, 214.5474525 ± 8.729604573, 207.3446553 ± 7.46713425 and 219.1978022 ± 8.291009297 respectively. The number of hydrogen bonds formed between the target enzyme and analogues was 2.934065934 ± 1.31516096, 1.23976024 ± 1.145625394 and 2.094905095 ± 0.839037553 for M10, M23 and M32 respectively (Fig. 7**B**).

4. Discussion

Here, we used an X-ray crystal structure of the main protease enzyme complexed with masitinib (PDB ID: 7JU7) for the structure-based identification of inhibitor analogues. Masitinib is an orally available c-kit inhibitor that has been approved in dogs for the treatment of mast cell malignancies (Dubreuil et al., 2009; Hahn et al., 2008) and is currently being evaluated in humans for Alzheimer's disease, cancer, multiple sclerosis, and amyotrophic lateral sclerosis (Hahn et al., 2008; Mora et al., 2020; Ottaiano et al., 2017; Vermersch et al., 2012). Masitinib works as a competitive inhibitor of M^{pro}, according to a recent study, and treatment of masitinib in mice infected with SARS-CoV-2 results in a 200-fold reduction in viral titers in the lungs and nose, as well as a reduction in lung inflammation. This inhibitor was likewise efficient *in vitro* against all of the reported variants of concern (B.1.1.7, B.1.351, and P.1) (Drayman et al., 2021). Given Masitinib's side effects, this research aims to substitute different chemical moieties for the inhibitor's *N*-methylpiperazine group and explore their toxicity using *in silico* approaches, as well as their binding to M^{pro} using a molecular docking and dynamics approach. A total of 18 analogues out of 39 have promising drug-like characteristics. The ability of the filtered drug-like analogues to bind and interact with the M^{pro} enzyme was investigated. The analogues M10 with methylamine moiety, M23 with morpholine substituent and M32 with 4-methylmorpholine group which were bound to the active-site pocket by hydrogen bonds and hydrophobic interactions, were selected as the best three analogues interacting with the target enzyme. Using MD simulations, the dynamic behaviour of the free M^{pro} enzyme and its complexes with analogues M10, M23, and M32 was investigated, and their stabilities were validated in terms of RMSD, Rg, SASA, and hydrogen bond number. Thus, the three analogues- M10, M23, and M32 not only have optimum drug-like qualities but also binds well to the target enzyme,

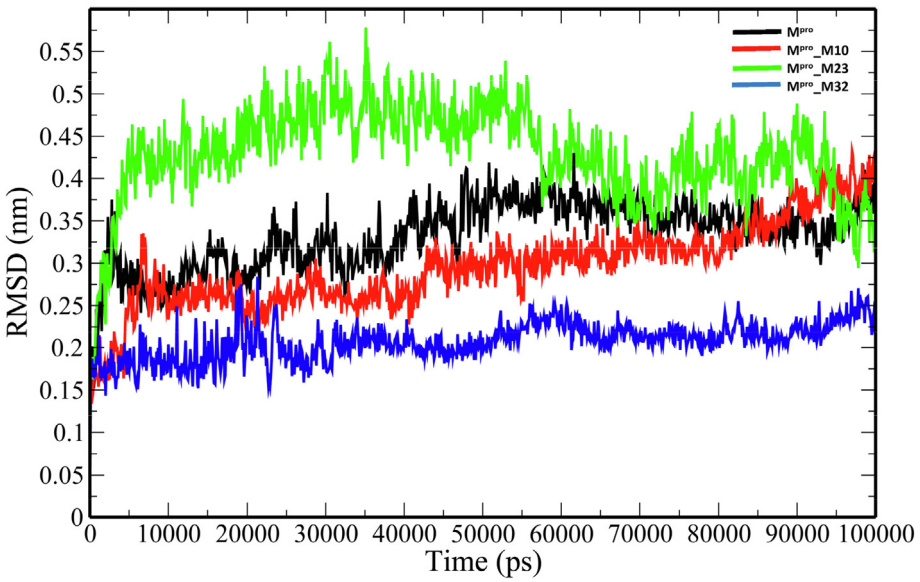

Fig. 3. The RMSD plot of backbone atoms of the unbound M^{pro} and M^{pro}-analogue complexes.

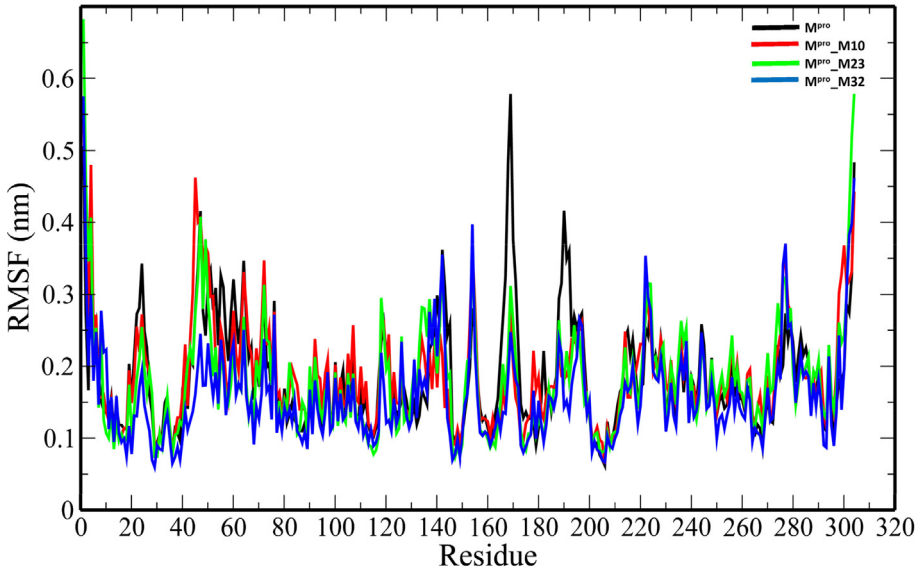

Fig. 4. The RMSF plot of backbone atoms of the unbound M^{pro} and M^{pro}-analogue complexes.

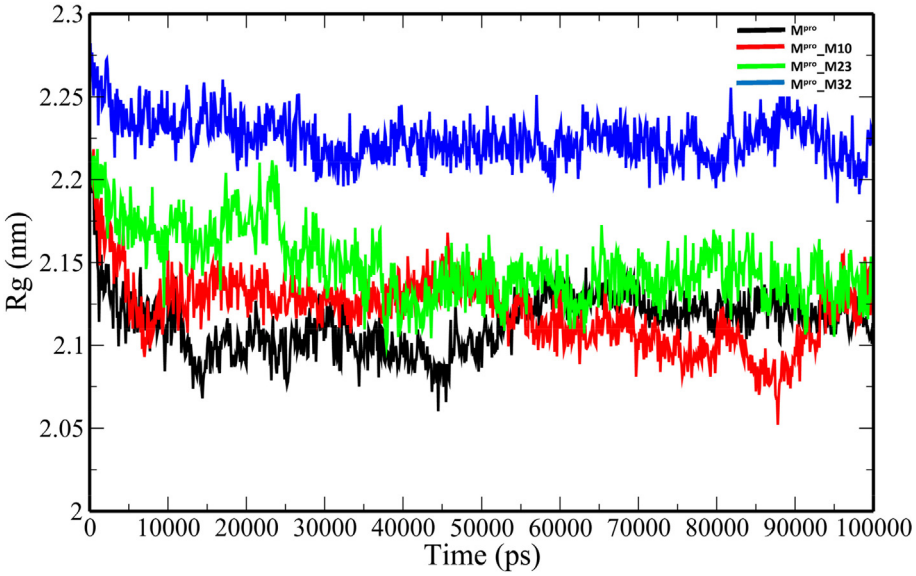

Fig. 5. The plot of Rg of the unbound M^{pro} and M^{pro}-analogue complexes.

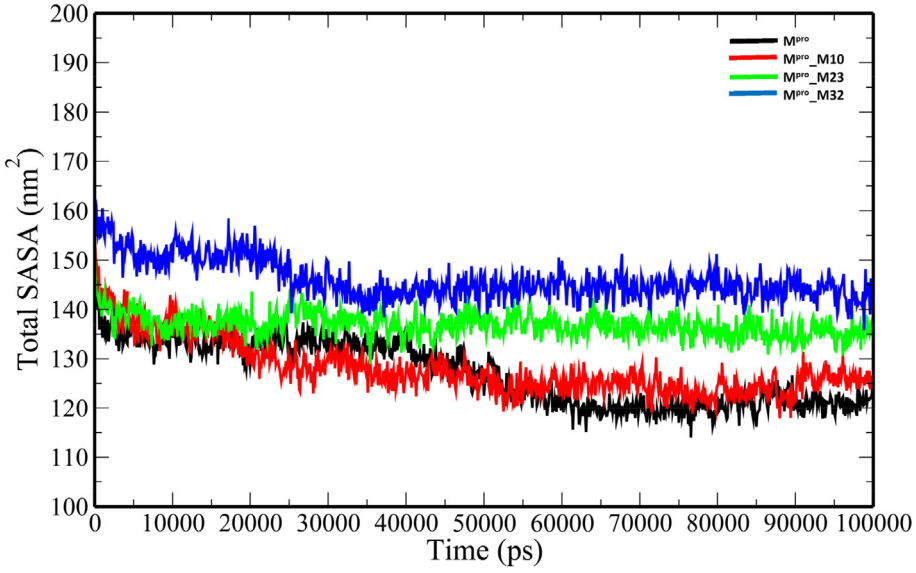

Fig. 6. The total SASA plot of the unbound M^{pro} and M^{pro}-analogue complexes.

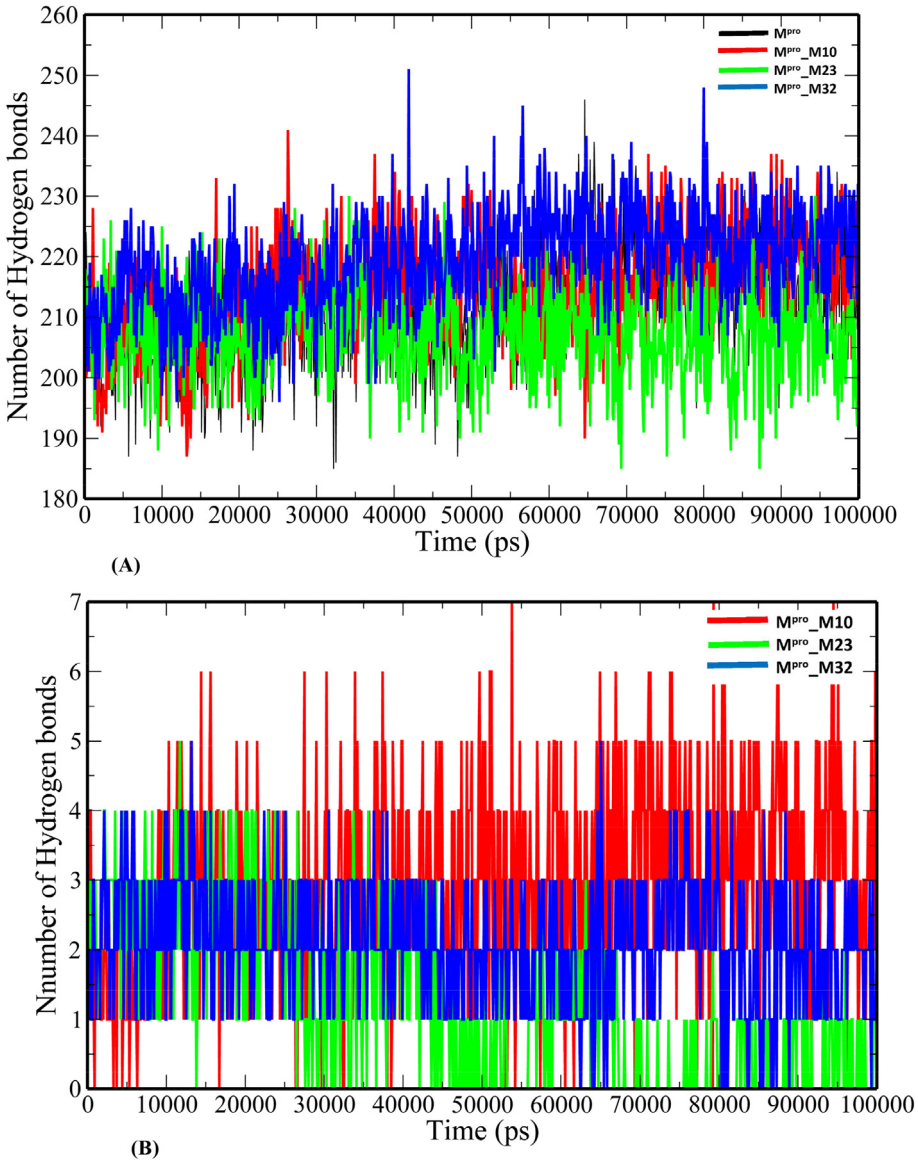

Fig. 7. The plot of number of hydrogen bonds versus time (A) intramolecular hydrogen bonds (B) intermolecular hydrogen bonds between M^{pro} and masitinib analogues.

indicating that they could be developed into SARS-CoV-2 drug candidates. It would also be fascinating to explore if these analogues can be developed into broad-spectrum inhibitors against the emerging coronavirus variants. While the preliminary findings are encouraging, the wet-lab experiments are required to establish the anti-SARS-CoV-2 effectiveness of the analogues.

5. Conclusion

The paucity of effective therapy, as well as the ongoing rise in fatality rates as new variants of SARS-CoV-2 arise, necessitating the discovery of innovative drug candidates. Using a combined technique of molecular docking and dynamics simulation, we studied the anti-SARS-CoV-2 potential of structural analogues of masitinib, an orally tolerable tyrosine kinase inhibitor that is now being investigated in clinical trials for numerous human disorders. We discovered three structural analogues-M10, M23 and M32 with significant binding affinities to the drug target enzyme SARS-CoV-2 M^{pro}. Our study suggests that the substitution of *N*-methylpiperazine group of masitinib with methylamine, morpholine and 4-methylmorpholine moieties enhances the affinity toward the target enzyme. Our findings will help in understanding the structure–activity relationship of these analogues and further need to be validated through wet-lab experiments.

Declaration of Competing Interest

The authors declare that they have no known competing financial interests or personal relationships that could have appeared to influence the work reported in this paper.

Acknowledgment

The authors extend their appreciation to the Deputyship for Research & Innovation, Ministry of Education in Saudi Arabia for funding this research work through the project no. (IFKSURG-2-286).

References

Anand, K., Ziebuhr, J., Wadhwani, P., Mesters, J.R., Hilgenfeld, R., 2003. Coronavirus main proteinase (3CLpro) structure: basis for design of anti-SARS drugs. Science (80-) 300, 1763–1767.

Berendsen, H.J.C., van Postma, J.P.M., van Gunsteren, W.F., DiNola, A., Haak, J.R., 1984. Molecular dynamics with coupling to an external bath. J. Chem. Phys. 81, 3684–3690.
Darden, T., York, D., Pedersen, L., 1993. Particle mesh Ewald: An N· log (N) method for Ewald sums in large systems. J. Chem. Phys. 98, 10089–10092.
Dubreuil, P., Letard, S., Ciufolini, M., Gros, L., Humbert, M., Castéran, N., Borge, L., Hajem, B., Lermet, A., Sippl, W., et al., 2009. Masitinib (AB1010), a potent and selective tyrosine kinase inhibitor targeting KIT. PLoS One 4, e7258.
Folch, J., Petrov, D., Ettcheto, M., Pedros, I., Abad, S., Beas-Zarate, C., Lazarowski, A., Marin, M., Olloquequi, J., Auladell, C., et al., 2015. Masitinib for the treatment of mild to moderate Alzheimer's disease. Expert Rev. Neurother. 15, 587–596.
Gurung, A.B., Ali, M.A., Lee, J., Farah, M.A., Al-Anazi, K.M., 2020. Unravelling lead antiviral phytochemicals for the inhibition of SARS-CoV-2 Mpro enzyme through in silico approach. Life Sci. 117831.
Hahn, K.A., Oglivie, G., Rusk, T., Devauchelle, P., Leblanc, A., Legendre, A., Powers, B., Leventhal, P.S., Kinet, J.-P., Palmerini, F., et al., 2008. Masitinib is safe and effective for the treatment of canine mast cell tumors. J. Vet. Intern. Med. 22, 1301–1309.
Halgren, T.A., 1996. Merck molecular force field. I. Basis, form, scope, parameterization, and performance of MMFF94. J. Comput. Chem. 17, 490–519. https://doi.org/10.1002/(SICI)1096-987X(199604)17:5/6<490::AID-JCC1>3.0.CO;2-P.
Hess, B., Bekker, H., Berendsen, H.J.C., Fraaije, J.G.E.M., 1997. LINCS: a linear constraint solver for molecular simulations. J. Comput. Chem. 18, 1463–1472.
Hess, B., Kutzner, C., Van Der Spoel, D., Lindahl, E., 2008. GRGMACS 4: Algorithms for highly efficient, load-balanced, and scalable molecular simulation. J. Chem. Theory Comput. 4, 435–447. https://doi.org/10.1021/ct700301q.
Hilgenfeld, R., Peiris, M., 2013. From SARS to MERS: 10 years of research on highly pathogenic human coronaviruses. Antiviral Res. 100, 286–295.
Humbert, M., De Blay, F., Garcia, G., Prud'homme, A., Leroyer, C., Magnan, A., Tunon-de-Lara, J.-M., Pison, C., Aubier, M., Charpin, D., others, 2009. Masitinib, ac-kit/PDGF receptor tyrosine kinase inhibitor, improves disease control in severe corticosteroid-dependent asthmatics. Allergy 64, 1194–1201.
Jin, Z., Du, X., Xu, Y., Deng, Y., Liu, M., Zhao, Y., Zhang, B., Li, X., Zhang, L., Peng, C., et al., 2020. Structure of M pro from SARS-CoV-2 and discovery of its inhibitors. Nature 582, 289–293.
Kathawala, R.J., Chen, J.-J., Zhang, Y.-K., Wang, Y.-J., Patel, A., Wang, D.-S., Talele, T.T., Ashby, C.R., Chen, Z.-S., 2014a. Masitinib antagonizes ATP-binding cassette subfamily G member 2-mediated multidrug resistance. Int. J. Oncol. 44, 1634–1642.
Kathawala, R.J., Sodani, K., Chen, K., Patel, A., Abuznait, A.H., Anreddy, N., Sun, Y.-L., Kaddoumi, A., Ashby, C.R., Chen, Z.-S., 2014b. Masitinib antagonizes ATP-binding cassette subfamily C member 10–mediated Paclitaxel resistance: a preclinical study. Mol. Cancer Ther. 13, 714–723.
Kim, S., Thiessen, P.A., Bolton, E.E., Chen, J., Fu, G., Gindulyte, A., Han, L., He, J., He, S., Shoemaker, B.A., Wang, J., Yu, B., Zhang, J., Bryant, S.H., 2016. PubChem Substance and Compound databases. Nucleic Acids Res. https://doi.org/10.1093/nar/gkv951.
Kneller, D.W., Phillips, G., Weiss, K.L., Pant, S., Zhang, Q., O'Neill, H.M., Coates, L., Kovalevsky, A., 2020. Unusual zwitterionic catalytic site of SARS–CoV-2 main protease revealed by neutron crystallography. J. Biol. Chem. 295, 17365–17373.
Laskowski, R.A., Swindells, M.B., 2011. LigPlot+: multiple ligand-protein interaction diagrams for drug discovery. J. Chem. Inf. Model. 51, 2778–2786. https://doi.org/10.1021/ci200227u.
Le Cesne, A., Blay, J.-Y., Bui, B.N., Bouché, O., Adenis, A., Domont, J., Cioffi, A., Ray-Coquard, I., Lassau, N., Bonvalot, S., et al., 2010. Phase II study of oral masitinib mesilate in imatinib-naive patients with locally advanced or metastatic gastro-intestinal stromal tumour (GIST). Eur. J. Cancer 46, 1344–1351.
Li, G., De Clercq, E., 2020. Therapeutic options for the 2019 novel coronavirus (2019-nCoV). Nat. Rev. Drug Discov. 19, 149–150.
Lipinski, C.A., 2004. Lead- and drug-like compounds: the rule-of-five revolution. Drug Discov. Today. Technol. 1, 337–341. https://doi.org/10.1016/j.ddtec.2004.11.007.
Mandal, A., Jha, A.K., Hazra, B., 2021. Plant Products as Inhibitors of Coronavirus 3CL Protease. Front. Pharmacol. 12, 167.
Mengist, H.M., Dilnessa, T., Jin, T., 2021. Structural basis of potential inhibitors targeting SARS-CoV-2 main protease. Front. Chem. 9.
Mora, J.S., Genge, A., Chio, A., Estol, C.J., Chaverri, D., Hernández, M., Mar\'\in, S., Mascias, J., Rodriguez, G.E., Povedano, M., others, 2020. Masitinib as an add-on therapy to riluzole in patients with amyotrophic lateral sclerosis: a randomized clinical trial. Amyotroph. Lateral Scler. Front. Degener. 21, 5–14.
Morris, G.M., Huey, R., Lindstrom, W., Sanner, M.F., Belew, R.K., Goodsell, D.S., Olson, A.J., 2009. AutoDock4 and AutoDockTools4: Automated docking with selective receptor flexibility. J. Comput. Chem. 30, 2785–2791. https://doi.org/10.1002/jcc.21256.
Ottaiano, A., Capozzi, M., De Divitiis, C., De Stefano, A., Botti, G., Avallone, A., Tafuto, S., 2017. Gemcitabine mono-therapy versus gemcitabine plus targeted therapy in advanced pancreatic cancer: a meta-analysis of randomized phase III trials. Acta Oncol. (Madr) 56, 377–383.
Papich, M.G., 2016. Masitinib Mesylate, in: Papich, M.G. (Ed.), Saunders Handbook of Veterinary Drugs (Fourth Edition). W.B. Saunders, St. Louis, pp. 476–477. https://doi.org/https://doi.org/10.1016/B978-0-323-24485-5.00355-7.
Riva, L., Yuan, S., Yin, X., Martin-Sancho, L., Matsunaga, N., Pache, L., Burgstaller-Muehlbacher, S., De Jesus, P.D., Teriete, P., Hull, M.V., et al., 2020. Discovery of SARS-CoV-2 antiviral drugs through large-scale compound repurposing. Nature 586, 113–119.
Sander, T., Freyss, J., von Korff, M., Rufener, C., 2015. DataWarrior: an open-source program for chemistry aware data visualization and analysis. J. Chem. Inf. Model. 55, 460–473. https://doi.org/10.1021/ci500588j.
Schüttelkopf, A.W., Van Aalten, D.M.F., 2004. PRODRG: a tool for high-throughput crystallography of protein–ligand complexes. Acta Crystallogr. Sect. D Biol. Crystallogr. 60, 1355–1363.
Drayman, N., DeMarco, J.K., Jones, K.A., Azizi, S.-A., Froggatt, H.M., Tan, K., Maltseva, N.I., Chen, S., Nicolaescu, V., Dvorkin, S., others, 2021. Masitinib is a broad coronavirus 3CL inhibitor that blocks replication of SARS-CoV-2. Science (80-.). 373, 931–936.
Tong, L., 2002. Viral proteases. Chem. Rev. 102, 4609–4626.
Ullrich, S., Nitsche, C., 2020. The SARS-CoV-2 main protease as drug target. Bioorganic & Med. Chem. Lett. 127377.
Veber, D.F., Johnson, S.R., Cheng, H.-Y., Smith, B.R., Ward, K.W., Kopple, K.D., 2002. Molecular properties that influence the oral bioavailability of drug candidates. J. Med. Chem. 45, 2615–2623.
Vermersch, P., Benrabah, R., Schmidt, N., Zéphir, H., Clavelou, P., Vongsouthi, C., Dubreuil, P., Moussy, A., Hermine, O., 2012. Masitinib treatment in patients with progressive multiple sclerosis: a randomized pilot study. BMC Neurol. 12, 1–9.
Wu, C., Liu, Y., Yang, Y., Zhang, P., Zhong, W., Wang, Y., Wang, Q., Xu, Y., Li, M., Li, X., Zheng, M., Chen, L., Li, H., 2020a. Analysis of therapeutic targets for SARS-CoV-2 and discovery of potential drugs by computational methods. Acta Pharm. Sin. B.
Wu, F., Zhao, S., Yu, B., Chen, Y.-M., Wang, W., Song, Z.-G., Hu, Y., Tao, Z.-W., Tian, J.-H., Pei, Y.-Y., et al., 2020b. A new coronavirus associated with human respiratory disease in China. Nature 579, 265–269.
Yang, H., Yang, M., Ding, Y., Liu, Y., Lou, Z., Zhou, Z., Sun, L., Mo, L., Ye, S., Pang, H., et al., 2003. The crystal structures of severe acute respiratory syndrome virus main protease and its complex with an inhibitor. Proc. Natl. Acad. Sci. 100, 13190–13195.
Zhang, L., Lin, D., Sun, X., Curth, U., Drosten, C., Sauerhering, L., Becker, S., Rox, K., Hilgenfeld, R., 2020. Crystal structure of SARS-CoV-2 main protease provides a basis for design of improved α-ketoamide inhibitors. Science (80-.). https://doi.org/10.1126/science.abb3405.
Zhang, J., Zeng, H., Gu, J., Li, H., Zheng, L., Zou, Q., 2020a. Progress and prospects on vaccine development against SARS-CoV-2. Vaccines 8, 153.
Zhou, P., Yang, X.-L., Wang, X.-G., Hu, B., Zhang, L., Zhang, W., Si, H.-R., Zhu, Y., Li, B., Huang, C.-L., others, 2020. A pneumonia outbreak associated with a new coronavirus of probable bat origin. Nature 1–4.